Real-Time Systems, 27, 49–70, 2004

Classification of Steam Generator Tube Defects for Real-Time Applications Using Eddy Current Test Data and Self-Organizing Maps

ROBERTO N. DE MESQUITA rnavarro@ipen.br
Nuclear Engineering Center, Nuclear and Energetic Research Institute (IPEN) and Mechanical Engineering Department, University of São Paulo, São Paulo, Brazil

DANIEL K. S. TING dksting@ipen.br
Nuclear Engineering Center, Nuclear and Energetic Research Institute (IPEN), São Paulo, Brazil

EDUARDO L. L. CABRAL elcabral@usp.br
Mechanical Engineering Department, University of São Paulo, São Paulo, Brazil

BELLE R. UPADHYAYA bupadhya@utk.edu
Nuclear Engineering Department, The University of Tennessee, Knoxville, USA

Abstract. A new classification method, for isolating steam generator tube defects in nuclear power plants using Eddy Current Test (ECT) signals, has been developed. The method uses Self-Organizing maps (SOM) with different data signatures to identify and classify these defects. A multiple inference system is proposed which evaluates different extracted characteristic SOMs to infer the defect type. Wavelet zero-crossing representation, a linear predictive coding (LPC), and other basic signal representations, such as magnitude and phase, are used to construct characteristic vectors that combine one or more of these features. These vectors are evaluated for their ability to classify tube defects and the ones with the best performance are used in the multiple inference system. The effectiveness of the method is demonstrated by applications of the characteristic maps to ECT data from various cases of tube defects in pressurized water reactor plant steam generators. The developed algorithm enables real-time applications such as fast tube defects classification systems and visualization of ECT signal feature prototypes, which may improve the speed of time-critical decision making during power plant maintenance outages.

Keywords: eddy current, self-organizing map, tube defects, nuclear plant

1. Introduction

Steam generators (SGs) are important components of pressurized water reactor (PWR) power plants. The U-tube steam generators (UTSG) in a typical 1300 MWe PWR have about 4000 tubes. The efficiency of a steam generator depends on the heat-transfer properties from the primary to the secondary fluid. This performance is significantly affected when a fraction of these tubes have to be plugged due to defects or because of degraded heat-transfer characteristics caused by tube fouling and deposits. The degradation of steam generator tubing (SGT) occurs by different mechanisms such as chemical corrosion, stress, deposits, mechanical fretting, or a combination of these.

Eddy Current Test (ECT) has been used for many decades as a standard non-destructive examination (NDE) technique for periodic maintenance of SGT structure.

Acquisition and processing of ECT data in nuclear power plants use automated and sophisticated technology to control ECT probe displacement and its positioning in tubes. Although most data processing and visualization is automated using commercial software, the data analysis is performed manually, off-line by several groups of specialists. Critical decisions have to be made regarding tube plugging, continued operation, or plant shutdown. This decision may have to be made in a short time when the plant is down for refueling or other scheduled maintenance.

The ECT analysis consists of comparing the obtained signals with a database of previous defect signals under similar conditions and for similar power plants. The implicit error range in this diagnostic methodology introduces a conservative view in making decisions about, for example, plugging a certain percent of tubes. This results in reduced equipment life and capacity. The automation of ECT data analysis is part of an effort to provide information on-line, and improve its overall performance through a predictive maintenance program.

The most important task in improving the automation of SGT ECT diagnostics is the development of a defect classification algorithm. Classical manual classification is usually based on the knowledge of probable locations of tube defects, power plant vendor, and the frequency channels that contain significant defect information.

Since the early 1990s, several methods have been proposed that could be used as auxiliary tools to ECT data analysis and future diagnostics automation (Udpa and Udpa 1990; Upadhyaya et al., 1993; Kurtz et al., 1996; Kang et al., 1998). The defect classification algorithm is the core of any reliable automated diagnostics system. Since the design and fabrication of steam generators vary from vendor to vendor, it is necessary to develop this technology using the knowledge base for each type of steam generator. Most of the contributions to ECT classification used calibration data, and were directed towards defect depth estimation.

Brown (1985) described a classification algorithm based on template matching using Fourier descriptors (Udpa and Lord, 1984) of ECT bobbin coil data. There is an oral presentation (Shindo et al., 1985) where microcomputer is said to be used to pre-process and classify data but without describing methodologies. A systematic attempt in classifying different defect types using artificial neural networks was presented by Udpa and Udpa (1990). The defects were separated as through wall hole defect, axisymmetric outer crack slot, flat-bottomed hole and axisymmetric inner defect slot. The neural network uses Fourier descriptors as inputs using 40 pattern vectors for training. The test set has 21 vectors. The neural network classifier is compared with a K-means clustering algorithm and it is said to have better results. Although the results were encouraging, possible automated application to field data needs further study.

Upadhyaya et al. (1993) were the pioneers in proposing a whole automated diagnostic system that included pre-processing, decoding, calibration, signal filtering, defect detection, feature extraction, type classification, and depth estimation. This system was based on a fuzzy inference system to classify the detected defects. Fuzzy rules were constructed for each test frequency and the range of defect size as indicated by each frequency.

Different feed-forward neural networks with three layers to estimate defect depth were also tested during late 1990s (Yan and Upadhyaya, 1996). These attempts were based on

a typical defect type (pitting) using 80 inputs, 50 neurons in the second layer, and 1 output. The author also used probabilistic neural networks to classify three different artifacts: tube support plate, ferrite, and copper. Wavelet zero-crossing representation was also introduced for ECT characterization (Yan and Upadhyaya, 1996; Upadhyaya et al., 1999).

Dodd (1996) described an approach to use neural networks to estimate defect depths using multi-frequency ECT signals. The signals from different frequency channels were used directly as input to a feed-forward neural network.

Another approach was developed by the ANL Steam Generator Integrity Program (Diercks et al., 1997). This report describes the estimation of defect depths using tube specimens that are produced at Pacific Northwest National Laboratory (PNNL) and metallographically analyzed. The primary defect type analyzed was inter-granular attack (IGA). The same work (Diercks et al., 1997) describes ultrasound techniques to estimate defect depth by ultrasound time of flight. Artificial neural networks were used for depth estimation. The PNNL approach (Kurtz et al., 1996) quantifies the defect size by regression models.

Shyamsunder group (Shyamsunder et al., 1995, 2000; Rao et al., 2002) has developed a comparative study of statistical methods and different artificial neural networks to classify produced or induced defects on stainless steel plates. The results show better efficiency of neural network methods over conventional statistical methods for classifying defect types. Authors cite difficulties on detection and characterization of fuel cladding tubes due to low signal-to-noise ratio in their engineering case study (Shyamsunder et al., 2000). Kohonen neural network is used only as a clustering technique.

Petri et al. (2000) have estimated the burst pressure from 14 tubes from its ongoing steam generator tube integrity program using a signal deconvolution technique associated with neural network. Numerical simulation databases have been used to inverse problem solution using neural networks (Zaoui, 1997; Chady et al., 2000; Simone and Morabito, 2001; Khandetsky, 2002).

Upadhyaya's group (Yan and Upadhyaya, 1996; Upadhyaya et al., 1999; Hooper and Upadhyaya, 1998) developed fuzzy inference systems with a set of rules based on signal characteristics with important results. The rules though, had to be manually configured by the user for each defect type detection and classification.

The research presented in this paper develops a new classification method that tests and compares different feature extraction techniques on actual nuclear power plant data pre-classified by certified ECT inspectors. A set of characteristics vectors composed of one or more signal-extracted features are used as input to obtain two-dimensional self-Organizing maps (SOMs) for each characteristic signature vector. These maps are obtained using a modified Kohonen algorithm with smooth supervision and are compared and evaluated taking into consideration their ability to classify tube defects. Thus, optimal feature maps are used as input to a multiple inference system. This classification algorithm does not take into consideration other related information such as defect localization in tube, excitation frequency channel, or the type of SG. Only information that comes from the signal itself is used. This method can contribute to ECT signal modeling problem as it objectively measures the importance that signal intrinsic features have on their characterization.

2. Eddy Current Testing

The principle of ECT is based on the electromagnetic interaction between a bobbin coil and an electrically conductive specimen (Figure 1). The probe consists of a coil that is subject to alternating electromagnetic field (primary field) that induces circular currents in the sample. These circular-trajectory currents occur in planes perpendicular to the primary field and are referred to as eddy currents. The eddy currents generate a secondary electromagnetic field (secondary field) that opposes the primary field. The interaction between the primary and the secondary fields results in an overall magnetic flux reduction in the coil. The bobbin coil complex impedance changes in accordance with eddy current redistribution due to material defects or non-homogeneities (Rajesh et al., 1993; McMaster, 1995).

ECT electromagnetic phenomenon can be described as static if displacement current is not considered (Equation (1)).

$$\nabla \times \left(\frac{1}{\mu} \nabla \times \mathbf{A} \right) = \mathbf{J}_s - j\omega\sigma\mathbf{A} \tag{1}$$

$\mathbf{J}_s$ is the source current density, $\mathbf{A}$ is the magnetic potential vector, μ is the magnetic permeability, σ is the material conductivity and ω is the excitation frequency. For a homogeneous medium Equation (1) can be rewritten as (Rajesh et al., 1993):

$$\frac{1}{\mu} \nabla^2 \mathbf{A} = j\omega\sigma\mathbf{A} - \mathbf{J}_s \tag{2}$$

The bobbin impedance changes are translated into electric potential variations. The ECT equipment usually represents these complex impedance variations by two signal components: resistance and inductive reactance. Traditionally, the impedance plane trajectories are used to characterize the defect.

The eddy currents depend on three different material characteristics of the sample. These are: geometry, electrical conductivity, and magnetic permeability. An important

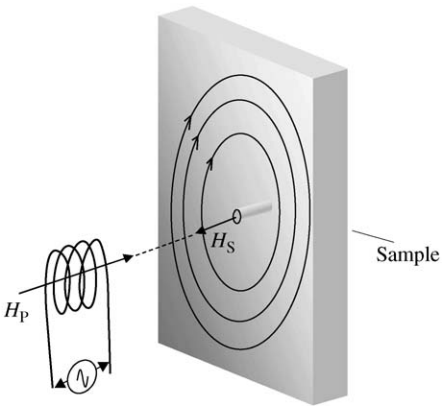

Figure 1. Electromagnetic interaction between bobbin coil and conductive sample.

electromagnetic property of this method is described by the skin depth, which can be obtained by the solution of the simplified diffusion equation and is given by:

$$d = \frac{1}{2\pi \left(\mu_{\text{rel}}\, \sigma\, f\ 10^{-7}\right)^{1/2}} \tag{3}$$

where d is the electromagnetic penetration depth and f is the ECT frequency. This ECT property is reflected in the phase rotation phenomenon where the impedance plane phase increases as the penetration depth increases. By using this property, the defect depth estimation can be made after appropriate phase calibration. A common technique in ECT inspection of SG tubes is the multi-frequency analysis in which a single probe stimulates the sample with different excitation frequencies in order to detect defects at different depths.

Typical SG tube defects may be established based on system knowledge. These are: cause of degradation, plant type in which tubes are located, and defect localization in the tube. This work uses degradation cause criterion, which was embedded in a database (such as EPRI's Performance Demonstration Database—PDD (EPRI, 1995)). Degradation can be divided into two categories: mechanical causes and chemical causes. The main degradations due to chemical causes are: thinning (THI), pitting (PIT), inter-granular attack (IGA), stress-corrosion cracking (SCC), inter-granular attack and simultaneous stress-corrosion cracking (ISC). The primary degradations due to mechanical causes are: wear (WEA), impingement (IMP), and fatigue.

Thinning is a generic term that refers to volumetric material loss. The local chemical conditions are altered before corrosion begins. The attack initiates by the surface material dissolution. There is no evidence of granular border attack. This defect is generally found near the tube support plate and other support structures.

The IGA plus SCC is a generic description for a degradation caused by a combination of factors: susceptible material, corrosive chemical conditions, and localized stress. The IGA alone has volumetric shape and is caused by a uniform grain border attack. SCC consists of multiple cracks with inter-granular propagation.

Impingement is a specific degradation type caused by suspended solids that impact tube surface, which often occurs in once-through steam generators.

Wear is a degradation caused by the impact of a spurious object or tube interaction with support structure. The associated morphology depends on the shape of the impacting agent.

Pitting defect is due to a general corrosion or due to local galvanic differences with acid attacks by copper compounds. It assumes volumetric geometry without granular-border attack and has a limited extension (approximately 0.1 inches).

3. Self-Organizing Maps

The SOMs are neural networks that generate non-linear data mapping to a low-dimensional and regular matrix (Kohonen, 1982). They can be described as neural

networks with only one layer and a high degree of lateral interconnection. The self-organizing term describes its ability to non-supervised learning.

Some important SOM applications in signal classification have been published. The real first ones were voice (phonetic) signal patterns by Kohonen (1982) himself. Other important application for signal classification was imaging and manuscript character clustering (Kennedy and Morasso, 1990; Chiueh et al., 1994). Chromatographic systems are also classified using Kohonen maps (Debeljak et al., 2001) and classification of radar signals using Linear Predictive Coding (LPC) coefficients and SOMs (Sadjadi et al., 2000).

These networks use lateral inhibition that varies connection strengths between the map units in inverse proportion to the topological distance. This procedure moderates competition among neurons. The input space distribution is ordered based on an association between the input vectors $\mathbf{x}_j$ and the prototype vectors $\mathbf{p}_j$:

$$\mathbf{x}_j = \{z_1, z_2, \ldots, z_n\},\ z_i \in \Re \tag{4}$$

$$\mathbf{p}_j = \{\alpha_1, \alpha_2, \ldots, \alpha_n\},\ \alpha_i \in \Re \tag{5}$$

where $\{z_i\}$ are the input variables, n is the vector dimension; $\mathbf{x}_j \in \Re^n$ and $\mathbf{p}_j \in \Re^n$. Each input vector $\mathbf{x}_j$ has its corresponding prototype-vector $\mathbf{p}_j$. Each prototype-vector pertains to a bi-dimensional (or low-dimensional) map cell or node. Each cell prototype-vector is modified based on a distance definition between input and prototype vectors:

$$d(\mathbf{x}, \mathbf{p}_j) = \sqrt{(z_1 - \alpha_{1j})^2 + (z_2 - \alpha_{2j})^2 + \cdots + (z_n - \alpha_{nj})^2} \tag{6}$$

At each iteration t the nearest $\mathbf{p}_{ch}$ is the one with minimal distance to the vector where:

$$ch = \arg\min\{\text{dist}(\mathbf{x}, \mathbf{p}_j)\} \tag{7}$$

This chosen prototype is changed (and its neighbors) optimizing the distance measure. In a batch algorithm all cell nodes are updated by the nearest input vector. It has been proved that if $\mathbf{x}(t)$ and $\mathbf{p}_j$ are Euclidean vectors and a locally smoothed distance is used, the algorithm converges (Bouton and Pagès, 1992). The updating is based on Kohonen rule.

4. Supervised SOM

The SOM algorithm is usually taken as a non-supervised process, the same way traditional clustering methods are considered. In 1988, a small algorithm alteration was introduced by Kohonen for voice recognition application (''voice machine'') (Kohonen et al., 1984; Kohonen, 1988) where smooth supervision was taken into consideration during training phase, with similar classification results to those obtained many years later with Learning Vector Quantization (LVQ) (Kohonen, 2001).

In this algorithm variation, n-components were added at the end of the input vector, where n is the number of different classes to be recognized. Typical class vector

components are zeros and ones and therefore a vector $[0\,0\,0\,1\,0]$ would correspond to the fourth of five different classes. The training process consists of the following:

1. Codebook random initialization.

2. Choosing the ''best match unit'' (BMU) input vectors for each map unit.

3. Appending class vector components to the prototype-vectors.

4. In batch algorithm, all prototype vectors (whole map) are updated based on BMU's and in sequential algorithm, only one BMU is updated per iteration.

5. At the end of training, the algorithm chooses the corresponding label to be associated with each map unit that presents class vector components with greater value (between 0 and 1).

6. Final classification is done without using class vector components. The label associated with BMU is chosen for each test vector.

The small ''supervision weight'' on map organizing process can be estimated by the n/d_{len} ratio, where d_{len} is the training vectors length. If we have five different classes using feature vectors of dimension 128, this ''weight'' would be less than 4%. The vectors used for training can be seen as composed of two parts, $\mathbf{x}_a$ and $\mathbf{x}_c$. The first part, $\mathbf{x}_a$, refers to prototype vectors. The second part, $\mathbf{x}_c$, refers to the class of unitary vectors that have n-dimensions. The training vectors are concatenated vectors $\mathbf{x} = [\mathbf{x}_a\ \mathbf{x}_c]$ with $(n + d_{\text{len}})$ dimension. The codebook is updated based on Euclidean distances between the $\mathbf{x}$ vectors and input vectors, though the final classification only uses $\mathbf{x}_a$ distances. This ensures that most of the original SOM algorithm topological ordering is kept.

5. Methodology

In this research, a database called the Performance Demonstration Database (PDD) (EPRI, 1995) that contains multi-frequency ECT signals from tube defects was used. This database is used for training ECT inspectors, and present experimental ECT data from actual nuclear power plants and a coherent description of seven defect types associated with each signal.

The original database generally presented ECT signals acquired for a tube, and have approximately 30,000 sampled points corresponding to the total tube length (20–30 m). Each tube is submitted to multi-frequency tests, using four excitation frequency channels, where each channel presents a real signal (resistance) and an imaginary signal (inductive reactance). The data acquisition parameters are fixed: 4 different excitation frequencies (typical values are 600, 400, 200, and 100 kHz), sound displacement speed of 0.03 m/per second, digital sampling rate around 30 samples/inch. These values results in a sampling rate of 396 samples/second or 396 Hz. The data files contain 16 columns, corresponding

to real and imaginary parts of absolute and differential probes for each of the four excitation frequencies.

The database for training and test was composed of five different defect types, a set of 24 indications each. In order to keep equal number of different sample vectors for each defect type, five defect types were chosen: ISC, PIT, THI, WEA, and IMP. For each indication, ECT signals from two differential frequency channels were used. Therefore, 240 sample vectors were used to train and test the classification system. The train and test sets were constituted of 120 sample vectors each, picked randomly from PDD for each classification experiment, always keeping the same number of samples (24 samples) for each defect type.

Pre-processing phase included calibration, filtering, mixing, and normalization. The calibration assured that phase and magnitude of ECT signals were consistent with those for the measurements. Noise filtering was applied when necessary.

Mixing consists of subtracting two different excitation frequency signals in order to eliminate the artifact signal due to support structures. There are many mixing methods, but the most common approach uses scaling, rotation, and translation matrix (Stolte et al., 1982). This procedure was used for signals that presented defect indications very near to support structures, where a superposition of the defect and the artifact occurred. Mixing was applied to data related to impingement, to 40% of wear data and to 30% of thinning data. Two mixed signals were created in these cases: the first corresponds to the mixing of 400 kHz signal with 100 kHz signal, and the second corresponds to the mixing of 200 kHz signal with the 100 kHz signal.

The obtained vectors were normalized using maximum of complex plane modulus keeping Lissajous-type signal shape (Figure 2) in this plane as unchanged. This criterion made the classification task independent of the signal amplitude. This is justified for the sake of searching signal intrinsic patterns and shapes that usually are the basis for off-line analysis.

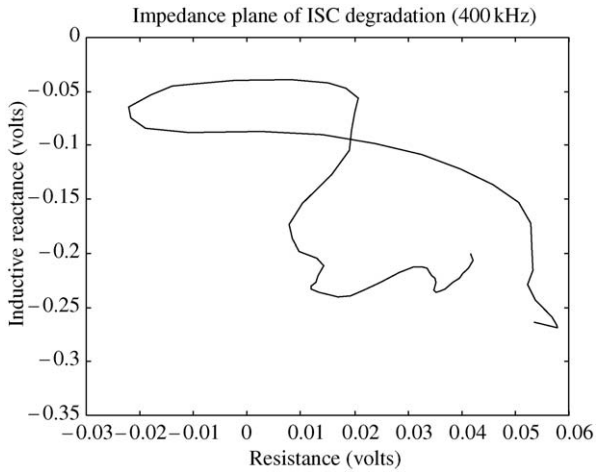

Figure 2. Typical impedance plane ECT signal showing ISC degradation.

6. Feature Extraction Methods

The following feature extraction methods were used to process input feature vectors to train the SOMs.

6.1. Signal Segmentation

Sets of different size (32, 64, 128 point) vectors were obtained by sampling around the defect center point. This point is equivalent to the median sample of the degradation area signal. The affected area generally contains 200–500 samples. Usually, this central sample contains the deepest degradation region and it is used for phase estimation. Figure 3 shows the segmentation method used for the sampled signal. The CI means central indication and is determined by the groups of specialists in PDD (EPRI, 1995).

6.2. Modulus

ECT signal modulus is a previously used feature (Upadhyaya et al., 1993; Yan and Upadhyaya, 1996; Hooper and Upadhyaya, 1998) for characterizing and classifying defects based on defect type and depth. This feature represents signal segment magnitude and is defined by the vector **C** modulus:

$$M = \|\mathbf{C}\| = \sqrt{R^2 + X_L^2} \tag{8}$$

where M is the modulus, R is the resistance and X_L is the inductive reactance.

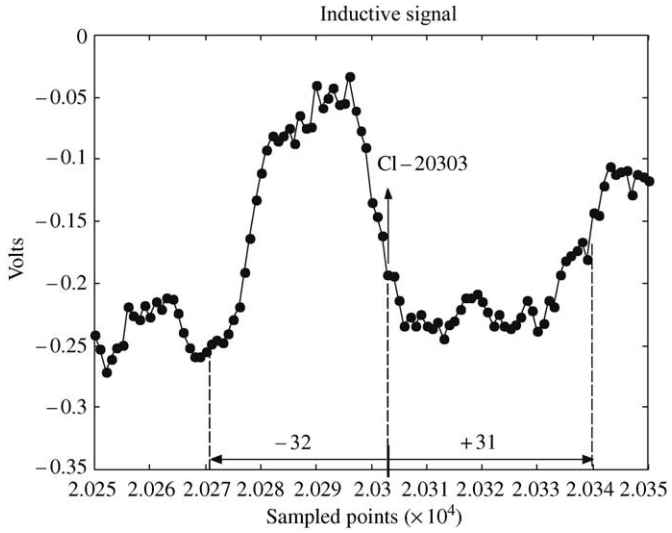

Figure 3. ECT signal segmentation criterion using CI (central indication) as reference.

In this work, the modulus feature vector is a 32, 64 or 128 point-vector constructed applying Equation (8) for each sample of segmented vector.

6.3. Phase

Phase is the main feature used during ECT inspection. The vectors are obtained from the ECT Lissajous figure formed in the impedance plane. It takes into account that the ASME calibration has been performed with 40° angle for a 100% through hole. The phase is defined as:

$$\varphi = \tan^{-1}\left(\frac{X_L}{R}\right) \tag{9}$$

The phase feature vector is obtained by applying Equation (9) for each sample of segmented vector.

6.4. Linear Predictive Coding

The LPC is a signal analysis technique mostly applied in speech recognition tasks (Rabiner and Schafer, 1978). The basic principle of this analysis is that the signal sample can be approximated as a linear combination of past samples. By minimizing the sum of squared prediction errors (over a finite interval) between the actual samples and the linearly predicted ones, a unique set of predictor coefficients can be determined. It has been used for feature extraction for signal recognition (Sadjadi et al., 2000) and image compression (Wade, 1993). An autoregressive one-step predictor model of a discrete signal $x(k)$ has the form:

$$x(k) = \sum_{i=1}^{n} a_i\, x(k-i) + w(k) \tag{10}$$

where a_i are the model parameters. The model parameters and the model order, n, are estimated using a least-squares technique. The sequence $w(k)$ represents uncorrelated noise. A detailed description of the LPC theory can be found in good review papers (Makhoul, 1975) and books on speech signal processing (Rabiner and Schafer, 1978).

The number of LPC coefficients used in this work was defined as 25% of the used segmented vector size that presented prediction error less than 15%. The prediction error used was the ratio between the mean squared error of predicted vector and the maximum error. The maximum error was the mean squared distance from segmented vector to zero axis. A typical LPC feature vector with 30 coefficients corresponding to an ISC degradation is shown in Figure 4.

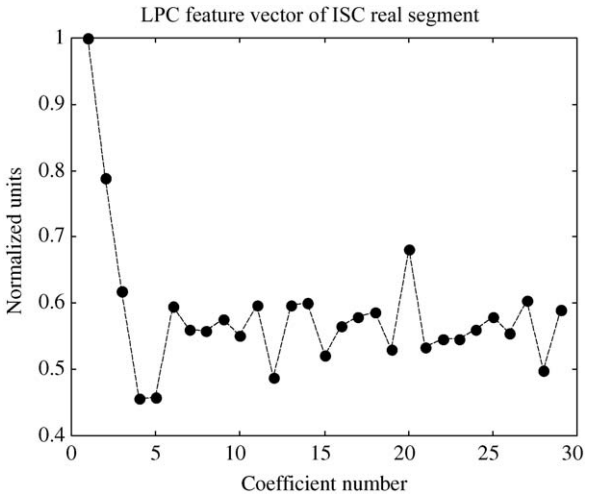

Figure 4. A typical LPC feature vector with 30 coefficients for an ISC degradation indication.

6.5. Wavelet Zero-Crossing

The wavelet transform is a linear operation that decomposes the signal into different scale components. This transform is based on signal convolution with a dilation filter. The wavelet is defined as a function $\Psi(x) \in L^2$, where L^2 is the Hilbert space (Young, 1988) and

$$\int_{-\infty}^{+\infty} \psi(x)dx = 0 \tag{11}$$

The wavelet transform of a function $f(x)$ in scale s and position x is given by the convolution product:

$$W_s^{\psi}(x) = f(x) * \psi_s(x) \tag{12}$$

Grossmann and Morlet (1984) showed that this transform satisfies an energy conservation equation and that $f(x)$ can be reconstructed from its wavelet transform. When s decreases, the dilation transform $\Psi_s(x)$ decreases, $W_s(x)$ can be sensitive to smaller details of the signal. The s-scale describes the regularity and size of the signal extracted characteristics by the wavelet transform.

Mallat (1991) developed WZC method for characterizing transient signals. He showed that for a specific class of generating functions (wavelets), the number of zero-crossings of these transforms is related to the localization of the signal variations for different frequency scales. Mallat still developed the so-called ''wavelet zero-crossings (WZCs) representation'' which was shown to be well-suited for pattern recognition problems

(Mallat, 1991). This representation is based on evaluating the wavelet transform integration between each two consecutive zero-crossing points z_{n-1} and z_n:

$$c_n = \int_{z_{n-1}}^{z_n} W_{2^j}^{\psi} f(x)dx \tag{13}$$

The significant singular points are common to all dyadic scales (2^j). The local maximum amplitudes relate to the discontinuity type (Upadhyaya et al., 1999). If singularity amplitude is bigger than background noise it is possible to separate both as the singularity amplitude decreases slower than noise amplitude when the scale increases. In this way, the number of discontinuities can characterize the signal regularity. Zero-crossing localization in wavelet representation can be considered as the inflection points of the original signal. Depending on the number of scales of wavelet transformation, a zero-crossing representation (Figure 5) can be obtained through four basic steps (Upadhyaya et al., 1999):

1. Symmetry operation on both signal extremes to avoid border distortion.

2. Multi-scale wavelet transformation.

3. Determination of zero-crossing points.

4. Evaluation of integrals between two adjacent zero-crossing points.

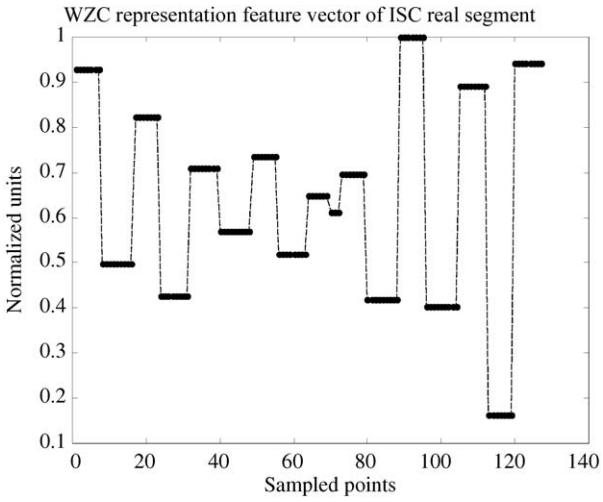

Figure 5. WZC feature vector with 128 sample points (ISC real signal segment).

7. Multiple Inference

We have developed an algorithm that uses multiple SOMs to infer a final class (Figure 6). The input vectors consist of a set of feature vectors. Each input vector with a different signal feature combination gives rise to a different SOM. Each of these maps is tested for their ability to classify defect types. The best-input vectors and their correspondent maps are chosen for use in the multiple inference system.

Multiple inference system is composed mainly of a set of selected pre-trained feature maps (Figure 6). The test vector is decomposed into corresponding features and BMU's from each map are found. As pre-trained maps have one label for each map unit, each map will produce one label for the tested vector. The final inference will be made under a selected criterion. The simple criterion considers the frequency of occurrence of label assignment. The more frequently assigned label for the test vector is chosen as the final label. This paper describes the results of using this simpler criterion. More information can be extracted from each feature map. The Euclidean distance from BMU's to test vectors and other similar information are the bases for other criteria that are being developed.

Each selected pre-trained map presents a codebook with different prototype clusters. For each feature map, each prototype cluster is related to a defect type. The codebooks of these maps constitute an implicit knowledge base representation and repositories that can be used for further classification efforts. This knowledge representation enable the

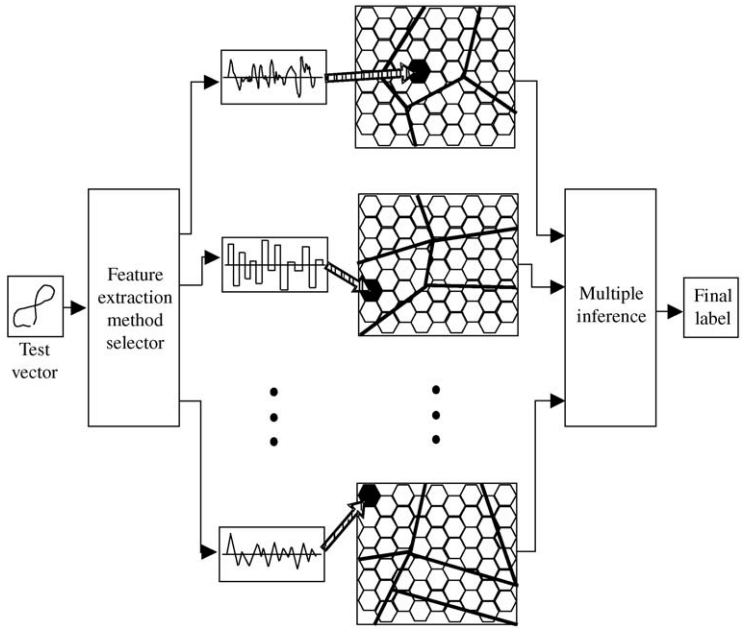

Figure 6. Multiple inference system.

visualization of prototype clusters and consequently, the possibility of checking by human specialists using this information.

7.1. Training Parameters

The SOM training algorithm was based on suggestions presented by Kohonen's Laboratory of Computer Information Science (LCIS, 2000) and is based on Matlab (The Mathworks, 2000). The training parameters were changed following three indices obtained during the process. The first index is called quantization error q_e, which measures the mean Euclidean distance between all training vectors and the respective BMU's prototypes. The q_e value is updated for each iteration. Activation distribution function determines the neighbor cells that are updated simultaneously in a batch training mode. The activation radius decreases during the training phase, which contains an approximate phase (with bigger radius) and a fine-tuned phase (with smaller radius).

Quantization error is the main map training quality index. In many cases, the number of map units is not big enough to represent data distribution and a relatively high training error may be obtained even with a longer training time. Kohonen (2001) establishes training parameters as:

$$m_{pd} = m_{\text{units}}/d_{\text{len}} \tag{14}$$

where m_{units} is the number of Kohonen map units and d_{len} is the number of training vectors. An empirical recommendation for the initial number of map units is:

$$m_{\text{units\_ini}} = 5 \cdot d_{\text{len}}^{0.54321} \tag{15}$$

Kohonen defines a ''small map'' as the one with $m_{\text{units\_ini}}/4$ and a ''big map'' as having $4 \cdot m_{\text{units\_ini}}$. This work uses ''big maps'' and two other sizes defined as ''huge'' $(12 \cdot m_{\text{units\_ini}})$ and ''super huge'' $(16 \cdot m_{\text{units\_ini}})$. These standard sizes are important to be defined in order to train many different feature maps without user intervention. Keeping the map size fixed for different training vector sets may make the training process less efficient and slower, as each training set (with different features) should have different sizes.

In this work, the first iterations would attain values near 4. The feature vectors are also normalized between 0 and 1. The recommended number of iterations (Kohonen, 2001) for typical maps is $50 \cdot m_{pd}$ where $10 \cdot m_{pd}$ for the initial phase and $40 \cdot m_{pd}$ for the fine-tuned phase. A typical map size used (32×19) to train 120 training vectors has m_{pd} of 5 approximately, though a recommended number of iterations will be 250. A short training number of iterations is defined as $50 \cdot m_{pd}/4$, or, for this example, 62 iterations.

The activation radius has decreasing ratio during training and its initial and final values are empirically defined. The initial recommended activation area (Kohonen, 2001) should occupy up to half the map area. This work adapted the initial radius as the fourth part of the number of units of the SOM matrix larger size. The map topographic was hexagonal, and for this, the topographic distances are equal in all directions. The final radius to define activation is one (first neighbors).

The second index was the topographic error (t_e). This error is defined as the ratio between the number of training vectors, for which the first and second BMU's were not first neighbors and the total number of training vectors. This error represents the topographic distribution preservation, which means a prototype distribution that represents data distribution. The third index used for choosing the training parameters was the classification index defined as:

$$\varepsilon = n_e/n_t \tag{16}$$

where n_e is the number of test vectors erroneously classified and n_t is the total number of test vectors.

The SOM size optimization through these three indices showed to be an important task. At first, bigger maps with long training time were trained to obtain reference values for q_e index. These values were used to obtain smaller maps with less training time, keeping the classification error as a final target. The quantization errors for the obtained maps varied between 0.001 and 0.5, and the topographic errors varied between 0 and 0.02.

8. Results of Application

This section presents the defect classification results using Kohonen maps with ''smooth'' supervision and multiple inference. Classification results are presented in Tables 1 and 2. Results are presented using the index for correct classification defined by:

$$\phi = 1 - \varepsilon \tag{17}$$

Each presented result (correct classification index) is the mean of ten different realized tests. Each test is done using a new random sampling from the database and a new training set. Mean right classification indices are presented with error range equal to standard deviation from all obtained results.

Tests were done using different signal segment sizes, (32, 64 and 128 sample points). The feature vectors listed in Tables 1 and 2 were constructed using these signal segments and results are shown for each of these feature vectors. Single feature vectors (using only one feature) and composed feature vectors as SRI (real and imaginary), PHM (phase and modulus), LRI (LPC coefficients of a SRI vector) and WRI (zero-crossings representation of a SRI vector).

Two training set sizes were used as input to the system. Table 1 presents individual maps inference results for a training set with 50% of database. Table 2 presents multiple inference results for a training set with 2/3 of database. The correct classification index has approximately 5% increase from Table 1 to 2.

From Table 1, classification results using LPC feature vectors and WZC feature vectors were 15 percentage points inferior to results obtained from direct signal segmentation feature vectors (like real segment or phase segment for instance).

Table 2 represents the combination of feature vectors with best results for multiple inference system. This combination includes five different maps: real and imaginary segment (SRI) map, real segment map (SRE) phase segment (SPH), phase and modulus (PHM) map, and Wavelet zero-crossings of real segment (SRW) map. This combination

Table 1. Correct classification index ($\phi = 1 - \varepsilon$) for Kohonen maps using different feature vectors from ECT signal.

	$(\overline{\phi} \cdot 100\% \pm 2\delta)$		
Feature vectors	128 points	64 points	32 points
Real segment	(72.0 ± 5.0)	(75.4 ± 3.5)	(73.3 ± 2.5)
Imaginary segment	(70.3 ± 4.5)	(71.2 ± 5.0)	(69.4 ± 3.5)
Real + imaginary	(76.0 ± 4.5)	(77.5 ± 2.5)	(78.3 ± 5.0)
Phase	(71.2 ± 3.5)	(72.5 ± 2.5)	(65.4 ± 3.5)
Modulus	(70.2 ± 4.5)	(71.5 ± 3.5)	(70.7 ± 4.0)
Phase + modulus	(77.4 ± 5.0)	(76.5 ± 4.0)	(74.3 ± 5.0)
LPC (real)	(51.2 ± 4.0)	(47.2 ± 3.0)	(45.4 ± 3.5)
LPC (imaginary)	(52.3 ± 3.5)	(46.4 ± 2.5)	(42.5 ± 4.0)
LPC (real + imaginary)	(61.6 ± 5.0)	(56.7 ± 5.0)	(55.4 ± 5.0)
WZC (real)	(51.4 ± 4.5)	(43.2 ± 4.0)	(38.4 ± 6.2)
WZC (imaginary)	(55.3 ± 5.0)	(45.4 ± 6.5)	(40.3 ± 5.0)
WZC (real + imaginary)	(58.5 ± 5.0)	(56.4 ± 6.0)	(46.2 ± 4.0)

of feature vector maps resulted in an increase in the correct classification index by about 5%.

A typical SRI trained map used for multiple inference is shown in Figure 7. This particular map yielded 92% correct classification index using 2/3 of database for training. This index was obtained for one specific random choice of training vectors with 128 sample points and a batch session of 1000 steps. The map presents 32 × 24 (768) map units, representing four times the number of sample-vectors used for training. The experiment as a whole made 10 trials for each of these combinations. The mean results are shown in Tables 1 and 2.

The codebook visualization is one important advantage of using Kohonen maps. As can be seen from Figure 7 the ordered map shows the more important Lissajous-type figures (patterns) for each defect type class. The map shows an organized prototype mapping which is representative of database distribution and useful for the classification task. Other representative prototype feature vectors were obtained as LRI and WRI maps.

Table 2. Correct classification index ($\phi = 1 - \varepsilon$) for multiple inference using five Kohonen maps with composed feature vectors from ECT signal.

	$(\overline{\phi} \cdot 100\% \pm 2\delta)$		
Multiple inference (SRI + SRE + SPH + PHM + SRW)	128 points	64 points	32 points
Train/Test (1/2 : 1/2)	(85.3 ± 4.5)	(83.7 ± 5.0)	(80.5 ± 5.0)
Train/Test (2/3 : 1/3)	(88.2 ± 3.5)	(87.5 ± 4.0)	(83.7 ± 4.5)

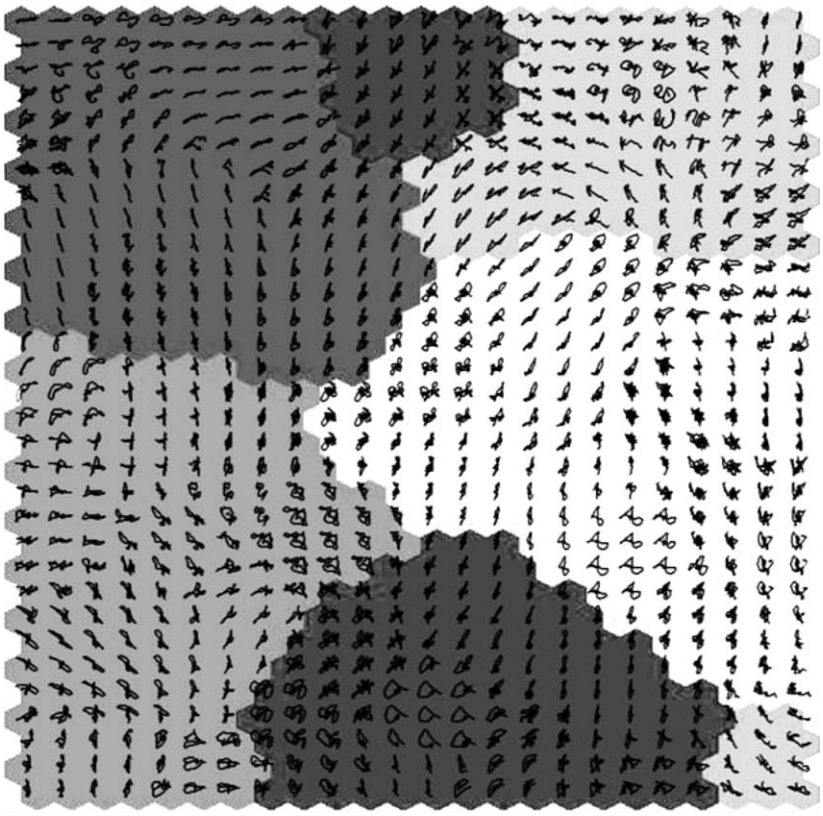

Figure 7. Approximate representation of SRI feature vector codebook superimposed on classified SOM map with a correct classification index of 92%. Background—crescent grayscale level representation for five different defect types: WEA (clearer), PIT, ISC, THI, and IMP (darker).

9. Concluding Remarks

A defect classification method for nuclear plant steam generators using ECT signal information was developed. Most previous classification methods were based on specific signal information such as tube localization, nuclear power plant type, and others.

The results of correct classification index for five different defect types have a mean value of 85% for multiple inference. This correct classification index is clearly better (approximately 5%) than the best results obtained for individual maps inference. Results showed that signal segment time representations are more important to signal classification than extracted features by wavelet zero-crossings representation and linear predictive coding coefficients. This can be attributed to the fact that the usual ECT signal (acquired during regular power plant inspections), that represents the degradation region, presents relatively few sampled points. However, these latter extracted features

can result in better classification indices (compared to individual feature results) if used in a multiple inference system (see Tables 1 and 2).

The method showed robustness considering the following aspects: it was tested for five different defect types; signal segmentation was based solely on center of degradation area; normalization was done using the impedance plane maximum modulus; and good correct classification indexes were obtained for 32-point sampled vectors.

The codebook maps can be used to estimate main signatures for each defect type. The method indicates excellent promise as an real-time classifier of tube defects. It also enables the visualization of feature vectors. The developed algorithm enables tube defects classification systems that would be an excellent operator aid in time-critical decision making during maintenance outages.

Acknowledgments

This research is sponsored by the Nuclear Engineering Center, IPEN, Brazil; partly supported by Conselho Nacional de Pesquisa, CNPq, under Grant No. 010005/98-2 and by International Atomic Energy Agency under project no. BRA/4/048. The research at The University of Tennessee is supported in part by the US National Science Foundation under Grant No. 9901201.

References

Bouton, C., and Pagès, G. 1992. Self-organization and convergence of the one-dimensional Kohonen algorithm with non uniformly distributed stimuli. *Laboratoire de Probabilités*. Université Paris VI, Paris.

Brown, S. D. 1985. Template matching—an approach for the machine sorting of eddy current data. *Materials Evaluation* 43(12): 1553–1565.

Chady, T., Enokizono, M., and Sikora, R. 2000. Neural network models of eddy current multi-frequency system for nondestructive testing. *IEEE Transactions on Magnetics* 36(4): 1724–1727.

Chiueh, T. D., Tang, T. T., and Chen, L. G. 1994. Vector quantization using tree-structured self-organizing feature maps. *IEEE Journals on Selected Areas in Communications* 12(9): 1594–1599.

Debeljak, Z., Strapac, M., and Medic-Saric, M. 2001. Application of self-organization maps for the classification of chromatographic systems and prediction of values of chromatographic quantities. *Journal of Chromatography A* 925: 31–40.

Diercks, D. R., Bakhtiari, S., Chopra, O. K., Kasza, K. E., Kupperman, D. S., Majumdar, S., Park, J. Y., and Shack, W. J. 1997. Steam generator tube integrity program. Semiannual Report, NUREG/CR-6511, ANL-96/17, v. 1, USA.

Dodd, C. V. 1996. Data analysis for steam generator tubing samples. Report for US. Nuclear Regulatory Commission, NUREG/CR-6455, ORNL/TM-13206.

EPRI—Electric Power Research Institute. 1995. Steam generator eddy current data analysis performance demonstration. Review material, Palo Alto, USA.

Grossmann, A., and Morlet, J. 1984. Decomposition of Hardy functions into square integrable wavelets of constant shape. *SIAM Journal of Mathematical Analysis* 15(4): 723–736.

Hooper, W. C., and Upadhyaya, B. R. 1998. An automated diagnostics system for eddy current data analysis of steam generator tubing. Annual Report of Nuclear Engineering Department of the University of Tennessee for the Electric Power Research Institute (EPRI).

Kang, S. J., Moon, J. C., Choi, D. H., Choi, S. S., and Woo, H. G. 1998. A distributed and intelligent system approach for the automatic inspection of steam-generator tubes in nuclear power plants. *IEEE Transactions on Nuclear Science* 45(3): 1713–1722.

Kennedy, J., and Morasso, P. 1990. Application of self-organizing networks to signal processing. *Lecture Notes on Computer Science* 412: 225–232.

Khandetsky, V., and Antonyuk, I. 2002. Signal processing in defect detection using back-propagation neural networks. *NDT & E International* 35(7): 483–488.

Kohonen, T. 1982. Clustering, taxonomy, and topological maps of patterns. In *Proceedings of the 6th International Conference on Pattern Recognition*. Munich.

Kohonen, T., Mkisara, K., and Saramki, T. 1984. Phonotopic Maps—insightful representation of phonological features for speech recognition. In *Proceedings of the 7th International Conference on Pattern Recognition*. Los Alamitos.

Kohonen, T. 1988. The neural phonetic typewriter. *Computer* 21(3): 11–22.

Kohonen, T. 2001. *Self-Organizing Maps*. Springer-Verlag.

Kurtz, R. J., Heasler, P. J., and Anderson, C. M. 1996. Performance demonstration tests for eddy current inspection of steam generator tubing. Pacific Northwest National Laboratory. Prepared for US Nuclear Regulatory Comission, NUREG/CR-6227, PNLL-9433, USA.

LCIS—Laboratory of Computer and Information Science. 2000. SOM Toolbox version 2. Finland (http://www.cis.hut.fi/projects/somtoolbox/).

Makhoul, J. 1975. Linear prediction: a tutorial review. *Proceedings of IEEE* 63(4): 561–580.

Mallat, S. 1991. Zero-crossings of a wavelet transform. *IEEE Transactions on Information Theory* 37(4): 1019–1033.

McMaster, R. C. 1959. *Nondestructive Testing Handbook*. Edited for the American Society for Nondestructive Testing, Ronald Press, New York.

Petri, M. C., Wei, T. Y. C., Kupperman, D. S., Reifman, J., and Morman, J. A. 2000. Eddy current signal deconvolution technique for the improvement of steam generator tubing burst pressure predictions. *Journal of Nondestructive Evaluation* 19(4): 149–164.

Rabiner, L. R., and Schafer, R. W. 1978. *Digital Processing of Speech Signals*. Prentice-Hall, New Jersey.

Rajesh, S. N., Udpa, L., and Udpa, S. S. 1993. Numerical model based approach for estimating probability of detection in NDE applications. *IEEE Transactions on Magnetics* 29(2): 1857–1860.

Rao, B. P. C., Raj, B., Jayakumar, T., and Kalyanasundaram, P. 2002. Using artificial neural network to quantify discontinuities in eddy current testing. *Materials Evaluation* 60(1): 84–88.

Sadjadi, M. R. A., Yao, D., Huang, Q., and Dobeck, G. J. 2000. Underwater target classification using wavelet packets and neural networks. *IEEE Transactions on Neural Networks* 11(3): 784–794.

Shindo, Y., Yoshie, S., and Marimoto, M. 1985. Quantitative system for evaluating eddy current testing of heat exchanger tubing. *Materials Evaluation* 43(10): 1299.

Shyamsunder, M. T., Rajagopalan, C., Ray, K. K., and Raj, B. 1995. A comparative study of conventional and artificial neural network classifiers for eddy-current signal classification. *Insight* 37(1): 26–30.

Shyamsunder, M. T., Rajagopalan, C., Raj, B., Dewangar, S. K., Rao, B. P. C., and Ray, K. K. 2000. Pattern recognition approaches for the detection and characterization of discontinuities by eddy current testing. *Materials Evaluation* 58(1): 93–101.

Simone, G., and Morabito, F. C. 2001. RBFNN-based hole identification system in conducting plates. *IEEE Transactions on Neural Networks* 12(6): 1445–1454.

Stolte, J., Udpa, L., and Lord, W. 1982. Multifrequency eddy current testing of steam generator tubes using optimal affine transformation. In *Review of Progress in Quantitative Nondestructive Evaluation*. New York: Plenum Press.

The Mathworks, 2000. Inc. Matlab version 5.3. USA.

Udpa, L., and Udpa, S. S. 1990. Eddy current defect characterization using neural networks. *Materials Evaluation* 48(3): 342–347.

Udpa, S. S., and Lord, W. 1984. A Fourier descriptor classification scheme for differential probe signals. *Materials Evaluation* 42(9): 1136–1141,

Upadhyaya, B. R., Yan, W., and Berkan, R. C. 1993. Hybrid digital signal processing and neural networks for automated diagnostics using NDE method. Annual Report of Nuclear Engineering Department of the

University of Tennessee for the US Nuclear Regulatory Commission Office of Nuclear Regulatory Research, USA.

Upadhyaya, B. R., Erbay, A. S., Hzi, G., and Sung, K. Y. 1999. Eddy current test data analysis for steam generator tubing diagnosis using artificial intelligence methods. Annual Report of Nuclear Engineering Department of the University of Tennessee for the Electric Power Research Institute (EPRI), USA.

Wade, M. A. 1993. Numerical study of linear predictive coding for the compression of gray scale images. M.Sc. Thesis, University of Tennessee, Knoxville.

Yan, W., and Upadhyaya, B. R. 1996. Development of an automated diagnostics system for eddy current analysis using applied artificial intelligence techniques. Annual Report of Nuclear Engineering Department of the University of Tennessee for the Electric Power Research Institute (EPRI), USA.

Young, N. 1988. *An Introduction to Hilbert Space*. New York: Cambridge University Press.

Zaoui, F., Marchand, C., and Razek, A. 1997. Localization and shape classification of defects using the finite element method and the neural networks. In *Proceedings of the 3rd International Workshop on E'NDE*. Reggio Calabria, Italy, September.

Roberto N. de Mesquita received his B.S. and M.Sc. degrees in physics from the University of Campinas (UNICAMP), Brazil in 1987 and 1991 respectively. He obtained his Ph.D. degree from the Mechatronic Engineering Department, University of São Paulo (USP), Brazil in 2002. Since 1991 he has been a faculty member at the Paulista University (UNIP), São Paulo. From 1995 to 1998 took part in the Boron Neutron Capture Therapy (BNCT) project at Nuclear and Energetic Research Institute (IPEN), São Paulo. Since 1998 he has participated in the project to develop an automatic system for monitoring and diagnosis of steam generator tubes in nuclear power plants, in cooperation with the Nuclear Engineering Department, University of Tennessee, Knoxville (USA), where he spent a year collaborating with Dr. Belle R. Upadhyaya. His current research interests are intelligent systems for pattern recognition on signals and applications such as monitoring and diagnosis of nuclear power plants and medical images.

Daniel K. S. Ting received his B.S. in Mechanical Engineering at the Escola Politécnica da Universidade de São Paulo in 1973, M.Sc. in Nuclear Engineering at the Escola Politécnica da Universidade de São Paulo, in 1976 and Ph.D. in Nuclear Engineering at the University of California, Berkeley in 1981. Between 1982 and 1994 he managed the project for the development and

construction of the reactor for a naval nuclear propulsion plant for the Brazilian Navy. In the period 1995–1999 he was the head of the Nuclear Engineering Department at the IPEN. Presently he is the head of the Monitoring and Diagnosis Division at IPEN. His main research interests are related to monitoring and diagnostic systems for nuclear power plants and he also teaches under graduated and graduated courses on nuclear power plants design.

Eduardo L. L. Cabral received the B.E. degree in mechanical engineering in 1982 from University of São Paulo, Brazil, the M.Sc. degree in nuclear engineering in 1985 from University of São Paulo, Brazil, and the Ph.D. degree in nuclear engineering from Massachusetts Institute of Technology in 1989. From 1989 to 1998 he was a senior engineer at the Energetic and Nuclear Research Institute, Brazil, where he worked on the Brazilian Nuclear Program. Since 1990 he has also been on the faculty of the Department of Mechanical Engineering at the University of São Paulo. His research interests include artificial neural networks, robotics, and system dynamics and controls.

Belle R. Upadhyaya received the Ph.D. degree in Systems Science from the University of California at San Diego. He is currently a Professor of Nuclear Engineering and College of Engineering Research Fellow at The University of Tennessee, Knoxville. His research interests include instrumentation and control, advanced signal processing, power and process plant monitoring and diagnosis, nondestructive examination, life prediction and aging of detectors and equipment, intelligent sensors, maintenance and reliability engineering. Dr. Upadhyaya has been the principal investigator of several research projects including power plant performance monitoring and advanced controls, signal validation, automated diagnosis of valve systems, nondestructive testing and fault diagnosis, aging studies of sensors and equipment, life prediction, and fault detection and isolation of sensors and field devices.

He has published over 220 articles in scientific journals and conference proceedings, chapters in handbooks, and is the author or co-author of over 100 research reports. Dr. Upadhyaya was a Visiting Research Scientist/Lecturer at Commissariat a L'Energie Atomique, Saclay, France; Netherlands Energy Research Foundation (ECN), Petten, The Netherlands; National University of Mar del Plata, Argentina; Electricite de France, Chatou, France; Instituto de Pesquisas Energéticas e Nucleares (IPEN), São Paulo, Brazil.